Electrical Tuning of the Fifth-Order Optical Nonlinearity of Antimony-Doped Tin Oxide

Ruipeng Hou,[#] *Hui Li*,[#] *Yanhui Sun*, *Mengjuan Diao*, *Ying Liang*, *Zhipeng Huang*,* *Jun Wang*, *Mark G. Humphrey*, *and Chi Zhang**

R. Hou, H. Li, Y. Sun, M. Diao, Y. Liang, Prof. Z. Huang, Prof. C. Zhang
School of Chemical Science and Engineering, Tongji University
Shanghai 200092, China
Email: zphuang@tongji.edu.cn; chizhang@tongji.edu.cn

Prof. J. Wang
Key Laboratory of Materials for High-Power Laser, Shanghai Institute of Optics and Fine Mechanics, Chinese Academy of Sciences
Shanghai 200092, China

Prof. M. G. Humphrey
Research School of Chemistry, Australian National University
Canberra ACT 2601, Australia

[#] Equal contributions
* Corresponding author: Zhipeng Huang, Chi Zhang

Keywords

Fifth-order nonlinear optics, nonlinear absorption, electrical tuning, tin oxide, liquid gate

Abstract

The electrical modulation of optical nonlinearity has gained extensive attention. However, most efforts thus far have been devoted to the nonlinear optical frequency

conversion of lasers, whereas the electrical tuning of nonlinear absorption remains rare. We demonstrate here the electrical tuning of the fifth-order nonlinear absorption of antimony-doped tin oxide (ATO) by ionic liquid gating. The fifth-order nonlinear absorption coefficient (γ_{eff}) of the ATO film can be monotonically modulated in the range 0.51 to 3.46 cm^3 GW^{-2}, with a maximum enhancement factor of 6.8. The electrostatic and electrochemical capacitance are responsible for the modification in the number of free carriers in the conduction band of ATO. The electrical modulation of the nonlinear absorption is ascribed to the voltage-dependent diameter of the undepleted core of ATO. A smaller voltage results in the charging of ATO and a larger undepleted core, and the size of the active component for three-photon absorption is larger. The electrochemical capacitance results from the chemisorption of H^+ and OH^- on the surface of the ATO, a larger water content in the ionic liquid affording a larger modulation range for the number of free carriers and the γ_{eff}.

1. Introduction

Electro-optical coupling devices working in the nonlinear optical (NLO) regime are attracting special attention, encouraged by potentially new approaches to optical signal processing. The electrical control of nonlinear generation has been recently implemented via plasmonic structures (e.g. gold nanoslits,[1] holey gold films,[2,3] gold nano-islands,[4] graphene nano-islands,[5] silicon metasurfaces[6]), two-dimensional (2D) layered structures (e.g. monolayer WSe_2,[7] monolayer MoTe,[8] bilayer MoS_2,[9] graphene[10]), CdS nanobelts,[11] organic conjugated polymers,[12] etc., but these

studies have focused on the electrical control of parametric NLO processes, e.g., second-harmonic generation (SHG) and third-harmonic generation (THG) of lasers.

Nonparametric NLO processes (e.g. nonlinear absorption and nonlinear refraction) comprise another important branch of nonlinear optics, one that has wide applications in advanced optical technologies including mode-locked lasers,[13,14] optical switches,[15,16] optical limiting,[17,18] bio-imaging,[19] etc. The electrical control of nonparametric NLO is therefore appealing, because this will possibly extend the procedures by which one can effect performance modulation as well as potentially expanding the types of NLO-based optoelectrical devices. However, the active control of nonparametric NLO processes is comparatively underdeveloped, despite extensive research concerning the steady-state nonparametric NLO behavior of materials,[20–22] limited examples including the electrochemical switching between (multiple) third-order NLO states of dipolar, quadrupolar, and octupolar organometallic molecules and dendrimers dispersed in solution;[23,24] however, it is difficult to envisage the integration of such compounds in on-chip applications.

Herein, we demonstrate the electrical tuning of the reverse-saturable absorption (RSA) of an antimony-doped tin oxide (ATO) solid thin film. The ATO film shows fifth-order nonlinear absorption with laser excitation at an incident wavelength of 1030 nm. The corresponding nonlinear absorption coefficient (γ_{eff}) can be monotonically modulated between 0.51 and 3.46 $cm^3\ GW^{-2}$ by external bias, using an ionic liquid (IL) as an electrolyte. Modulation of γ_{eff} by external bias is dependent on the size of the undepleted core of the ATO. Both electrostatic and electrochemical

processes (the chemisorption of H^+ and OH^- on ATO) occur during the variation of sample voltage. Water impurity in the IL is beneficial for effective charging/discharging, and therefore the modulation of nonlinear absorption. The results reported here suggest an effective and convenient approach for the controllable tuning of the NLO response of a material.

2. Results and discussion

2.1 Device structure

The NLO properties of a material are heavily correlated with the electronic states. Liquid electrolyte gating is efficient in modulating the carrier concentration in materials, because the capacitance is dictated by the electric double layer, decoupling the capacitance and the thickness of the electrolyte. Liquid electrolyte gating enables the conformal coating of materials, especially porous materials, and has been widely utilized to modulate various properties of materials, including conductivity,[25–27] ferromagnetism,[28–30] transmittance,[31,32] etc. In this work, the carrier concentration of a porous ATO film was modulated via electrolyte gating, and the corresponding NLO responses were investigated by an open-aperture Z-scan experiment (Figure S1 in the SI). The structure of the device is illustrated in Figure 1a. A nanoporous film of ATO was loaded on to a fluorine-doped tin oxide (FTO) substrate, to serve as the active material; an FTO substrate was used as the counter electrode, and an IL functioned as the electrolyte. The IL used here is 1-ethyl-3-methylimidazolium tetrafluoroborate (EMIM-BF_4). EMIM-BF_4 obtained from the supplier has a high

content of water (ca. 36,000 ppm), being a protic IL (PIL). The water content was reduced to 218 ppm after dehydration. Both hydrous and dehydrated EMIM-BF_4 were used in the experiment. The device filled with dehydrated EMIM-BF_4 is denoted as the IL device, and that with as-received EMIM-BF_4 as the PIL device. The carrier was accumulated or depleted in the ATO film by varying the applied voltage (V_A). Figure 1a shows an example where extra electrons are accumulated in the ATO film when a negative V_A is applied. With this modulation of the number of carriers in the ATO film, the NLO response of the ATO film could then be evaluated by Z-scan measurements at various V_A.

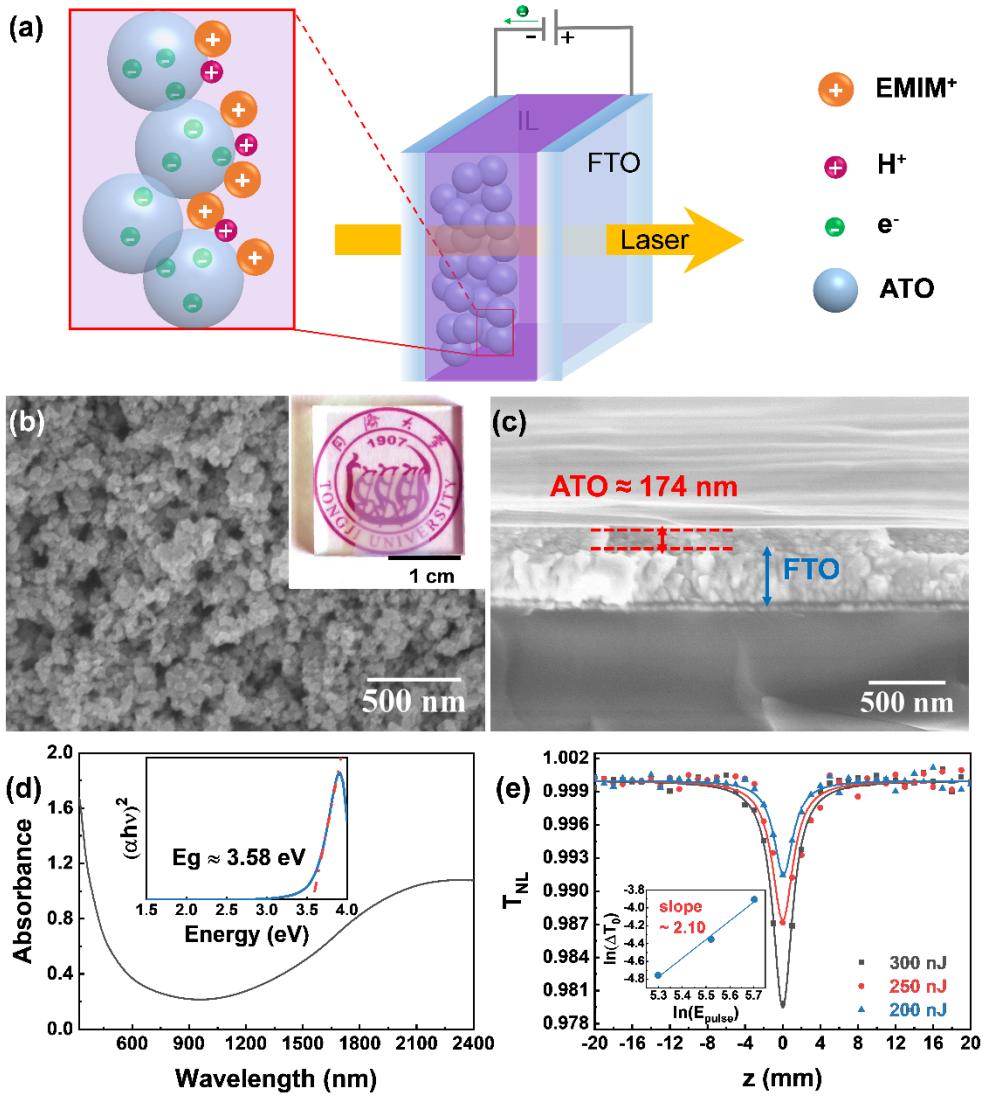

Figure 1. (a) Schematic structure of the device. (b) Plan-view SEM image of an ATO mesoporous film. The inset is a photograph of the ATO film on the FTO substrate. (c) Cross-sectional-view SEM image of an ATO mesoporous film. (d) Absorbance of the ATO film deposited on the FTO substrate; inset: the Tauc plot of the ATO film. (e) Open-aperture $T_{NL}(z)$ curves of the ATO film at 1030 nm with different pulse energies. The inset is the plot of $\ln(\Delta T_0)$ vs. $\ln(E_{pulse})$. The scatters are the experimental data, while the solid lines are the fitting results.

Commercially available ATO nanoparticles were used in our experiment. The survey XPS spectrum (Figure S2a in the SI) shows only signals from Sn, Sb, O, and C,

while the XRD pattern (Figure S2b in the SI) matches well with that from tetragonal phase cassiterite (JCPDS# 41-1445), confirming the composition and phase purity of the ATO. The average diameter estimated by the Scherrer equation[33,34] is 5.9 nm, consistent with those suggested by transmission electron microscopy (TEM) in Figure S2c in the SI. Energy-dispersive spectroscopy (EDS) indicates that the atomic ratio of Sn to Sb is 9.3:1 (Figure S2d in the SI). The ATO nanoparticles were deposited on to the FTO substrate by doctor blade deposition; the details of the film deposition can be found in the Experimental section. The morphology of the ATO film was investigated by scanning electron microscopy (SEM). Figure 1b shows that the film is a continuous spongy-like three-dimensional (3D) network. The pores in the 3D porous structure result from the thermal removal of the molecular structure scaffold (Carbowax 20000) during the thin film fabrication. The FTO substrate loaded with the 3D porous film of ATO appears faint blue in color and semi-transparent (inset of Figure 1b). The thickness of the ATO film is ca. 174 nm, according to a typical cross-sectional SEM image (Figure 1c). A camera image of an assembled device is shown in Figure S3 in the SI.

Figure 1d is a representative UV-Vis-NIR absorption spectrum of the ATO film on FTO, which was measured using bare FTO as background. The spectrum shows an absorption in the UV-Vis region, which is associated with inter-band excitations of the valence band electrons. A bandgap energy of 3.58 eV can be derived from a Tauc plot (inset of Figure 1d), which is similar to the reported bandgap of SnO_2 (3.67 eV)[35]. In addition to the interband absorption, another broad absorption is found near

2300 nm, which arises from localized surface plasmon resonance (LSPR) associated with the collective oscillation of free carriers in the conduction band of the ATO nanoparticles.[36]

The intrinsic NLO response of a pristine ATO film is shown in Figure 1e. The normalized transmittance of the ATO film (T_{NL}) decreases gradually when the sample is passed through the focal point of the laser, at which the position of the sample (z) is defined as zero (i.e., the normalized transmittance of the ATO film decreases with increasing laser intensity, characteristic of RSA behavior). The valley of the $T_{NL}(z)$ curve is deeper for larger pulse energies (200 to 300 nJ). In contrast, a bare FTO substrate shows a negligible NLO response under the largest laser pulse energy (Figure S4a in the SI), confirming that the RSA response comes from the ATO film but not the FTO substrate. The ln-ln scale plot of the normalized transmittance change (ΔT_0, the depth of $T_{NL}(z)$ curves' valley in Figure 1e) as a function of laser pulse energy (E_{pulse}) affords information about the nature of the nonlinear absorption; when the slope of the curve is (n-1), n is the effective number of photons absorbed.[37,38] Data fitting results in a slope of 2.10 for the ln-ln scale plot, suggesting that the RSA response is a nominal 3PA process, and therefore a type of fifth-order nonlinearity.

2.2 Electrical modulation of the NLO response

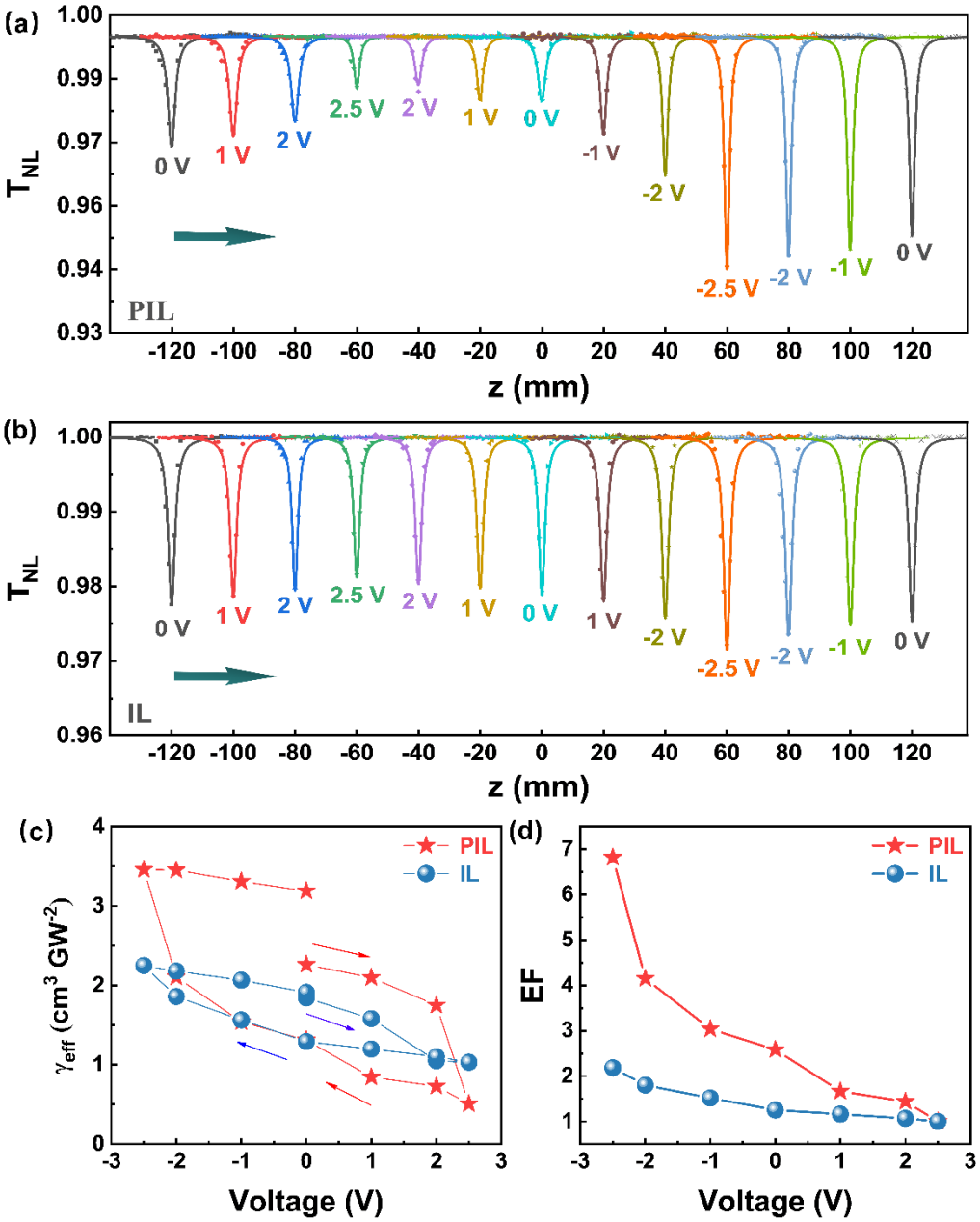

Figure 2. Open-aperture Z-scan curves of the PIL device (a) and the IL device (b) at 1030 nm with different voltages; the arrows indicate the direction of the voltage modulation. All scatters are the experimental data, and the solid lines are the fitting results. (c) γ_{eff} values of the devices corresponding to the different voltages. (d) EF plots of the two devices with the different voltages.

The electrical modulation of the NLO response of devices was investigated by Z-scan in the open-aperture configuration. Z-scan measurements were undertaken after a certain voltage was applied to the device for more than 1 minute, so that the electrical charging or discharging of the ATO reached an equilibrium state. The sequence of voltage steps applied to ATO is shown in Figure S5 in the SI. The corresponding $T_{NL}(z)$ curves are plotted in Figure 2a for the PIL device and Figure 2b for the IL device. The curves have been stacked with constant offset for convenience of comparison. The voltage was varied in the range 2.5 V to -2.5 V to avoid possible degradation of the EMIM-BF_4. All $T_{NL}(z)$ curves show a valley, indicating that smaller normalized transmittance corresponds to higher intensity laser flux at each focus (i.e., the NLO response is RSA in the two devices for all voltages).

The depths of valleys in the $T_{NL}(z)$ curves of both devices increase monotonically with decreasing voltage, confirming that the NLO response of the devices can be electrically modulated. In addition, the minimum of the $T_{NL}(z)$ curves of the PIL device (0.9456) is significantly less than that of the IL device (0.9776) at a voltage of -2.5 V, indicating that the modulation range of the NLO response of the PIL device is larger than that of the IL device. The same measurement was also carried out with a blank PIL device assembled by two bare FTO substrates. Under the same experimental conditions, the normalized transmittance of the blank PIL device lies between 99.5% and 100% (Figure S4b in the SI). The variation of $T_{NL}(z)$ for the blank PIL device is much smaller than that for a PIL device with the ATO film, confirming that the voltage-dependent RSA of devices comes exclusively from the ATO film.

The influence of voltage and electrolyte on the NLO response of the ATO film is further manifested by comparison of the fifth-order nonlinear absorption coefficients (γ_{eff}). The γ_{eff} values were derived from the $T_{NL}(z)$ curves by data fitting (Section 1 of the SI), the results being plotted in Figure 2c. The γ_{eff} of the PIL device can be monotonically modulated between 0.51 and 3.46 cm^3 GW^{-2}, with smaller γ_{eff} corresponding to larger voltage. The nonlinear absorption coefficient γ_{eff} in this work is comparable to those of semiconductors reported in the literature,[39–42] and indeed larger than most of them (Table 1 in SI). A clear hysteresis is seen in the γ_{eff}-V_A response that is characteristic of the PIL devices. With the same V_A, the γ_{eff} value corresponding to forward V_A modulation (from negative to positive) is larger than that corresponding to backward V_A modulation (from positive to negative). The IL device shows similar γ_{eff}-V_A behavior, but the modulation range and the hysteresis is smaller in comparison with the PIL device. The maximum γ_{eff} of the IL device is 2.25 cm^3 GW^{-2} for a V_A of -2.5 V, while the minimum γ_{eff} is 1.03 cm^3 GW^{-2} for a V_A of 2.5 V. The enhancement factor (EF) is defined as the ratio of γ_{eff} for a certain V_A to the minimum of γ_{eff}. The EF values of the PIL and the IL devices corresponding to forward V_A modulation are plotted in Figure 2d. The maximum EF is 6.8 for the PIL device, but only 2.2 for the IL device. The $T_{NL}(z)$ curves and γ_{eff}-V_A relationship demonstrate clearly that the NLO response of the ATO film can be effectively tuned by an applied voltage, and that PIL is more effective than IL for the electric control of γ_{eff}.

The EF of PIL-gated ATO is comparable to previously reported approaches to

effecting nonlinear absorption variation. One of us has reported third-order nonlinear absorption coefficient variation as a function of external stimulus for a series of Ru-based molecular inorganic compounds, and showed EF values in the range 2 - 10.[43–46] An 8-fold enhancement of third-order nonlinear absorption was achieved by protic switching of *trans*-[Ru(C=CHC$_6$H$_4$-4-NO$_2$)Cl(dppm)$_2$]PF$_6$ to *trans*-[Ru(C≡CC$_6$H$_4$-4-NO$_2$)Cl(dppm)$_2$].[47] Feng et al. have shown that a Rhodamine B salicylaldehyde hydrazone metal complex exhibits no NLO response, while the effective third-order nonlinear absorptive coefficient increases to -2.5×10^{-9} m W^{-1} after UV irradiation.[48] These reports focused on third-order NLO properties, while we have reported the modulation of the fifth-order NLO response in the present work. Furthermore, in these earlier reports, the molecules of interest are dispersed in solution for NLO performance modulation, but in the present work we have demonstrated the modulation of the NLO response of a solid thin film.

2.3 Voltage modulation

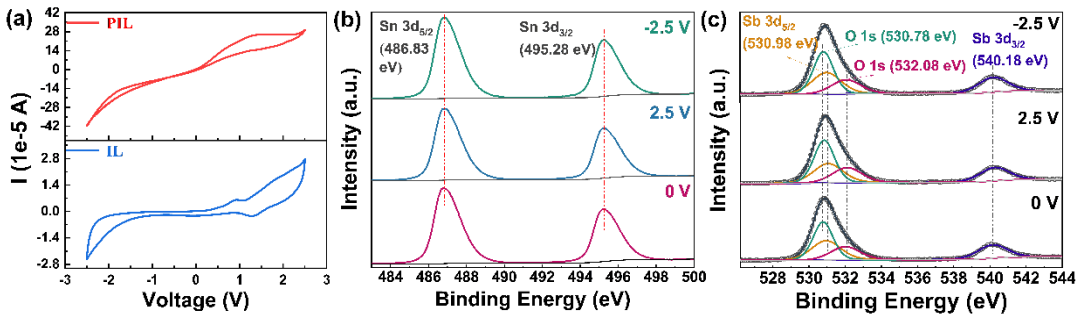

Figure 3. (a) Cyclic voltammograms of the PIL and the IL devices. XPS spectra of (b) Sn 3d, and (c) O 1s and Sb 3d windows of the ATO film in the PIL device after the application of voltage. The deconvoluted fitting results are shown for (c).

It has been reported that the OH^- and H^+ generated in the PIL from the H_2O can be chemically adsorbed on the surface of zinc oxide, with the corresponding cyclic voltammogram being unsymmetrical.[49] A typical cyclic voltammogram of the PIL device is shown in Figure 3a, which closely resembles that of PIL-gated zinc oxide. Two broad peaks near 0.9 V and 1.4 V were found, the former associated with chemical adsorption of OH^- on the surface of ATO, and the latter with water oxidation.[50] The cyclic voltammogram of the IL device was also measured (Figure 3a). An anodic peak associated with the chemisorption of OH^- was found, corresponding to residual H_2O impurity in the IL. At the same voltage, the current of the IL device is only one-tenth that of the PIL device, consistent with the much smaller water content of the IL (218 ppm) than the PIL (36,000 ppm).

X-ray photoelectron spectroscopy (XPS) was utilized to assess ATO under different V_A; if ATO undergoes redox processes, the binding energies of the metal ions will change, as has been reported for TiO_2 [51] and VO_2[52] under IL gating. The XPS spectra of PIL-gated ATO films subjected to voltages of -2.5, 0, and 2.5 V were monitored (Figure 3b and Figure 3c). The binding energy peaks at 486.8 eV and 495.3 eV arise from Sn $3d_{5/2}$ and Sn $3d_{3/2}$, respectively, and are typically assigned to the presence of Sn^{4+},[53] while the characteristic peaks at 530.9 eV and 540.2 eV correspond to Sb $3d_{5/2}$ and Sb $3d_{3/2}$, respectively.[54] The O 1s region was deconvoluted into several contributions. The lowest-energy peak 530.6 eV was assigned to metal (M)-O, while the next-lowest energy peak 532.1 eV was assigned to M-OH.[53] Comparison of the XPS spectra reveals no distinguishable shift in the

binding energies of Sb or Sn from samples subjected to the different voltages, suggesting that reduction and/or oxidation of ATO is unlikely to occur during the V_A modulation.

The cyclic voltammetry and XPS experiments suggest that both electrostatic and electrochemical processes occur during voltage modulation, with the electrochemical process associated with the chemisorption of H^+ and OH^- on the surface of ATO, but not the redox of ATO itself.

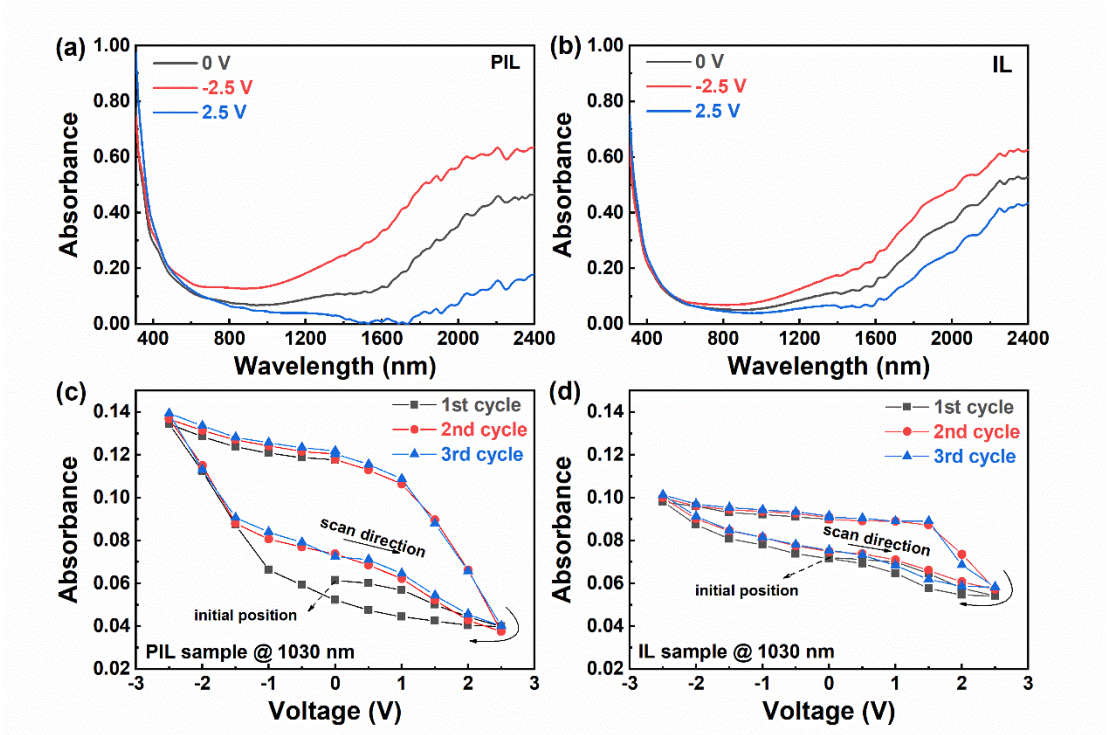

Figure 4. Absorbance spectra of (a) the PIL device and (b) the IL device with different voltages. The absorbance of the two devices at 1030 nm with different voltages is shown in (c) (PIL device) and (d) (IL device).

The linear absorption behavior of PIL and IL devices was monitored to understand the mechanism of the electrical modulation of the NLO response and the performance

difference between the PIL and IL devices. Figure 4a and Figure 4b show the absorbance spectra of the PIL device and the IL device, respectively, with different voltages. The two devices show a similar trend with the variation in voltage. Positive voltage decreases the LSPR absorbance near 2300 nm, while negative voltage increases the LSPR absorbance. The LSPR peak in the spectra of the ATO films in the PIL and IL devices persist with positive voltages, suggesting that the free carriers are not totally extracted from the conduction band of the ATO films under these conditions. Bare FTO substrates show no variation in the absorption spectrum (Figure S6 in the SI), so the variations in absorption can be exclusively associated with the ATO film in the devices. This behavior is in accordance with that of electrochromic devices using n-type transparent conductive oxide (TCO) nanoparticles as the active component.[36,55,56]

The linear absorbances of the two devices at 1030 nm were also monitored at the different voltages, the results being shown in Figure 4c and Figure 4d and the arrows indicating the direction of voltage modulation. The variation in absorption at 1030 nm is nearly identical across the voltage scanning rounds, indicating the repeatable nature of the modulation of absorption by voltage. For the PIL device, the variation of absorption at 1030 nm is up to 350%. For the IL device, the absorbance corresponding to the voltage of -2.5 V is nearly 190 % of that at 2.5 V.

2.4 Mechanism of electrical modulation of RSA

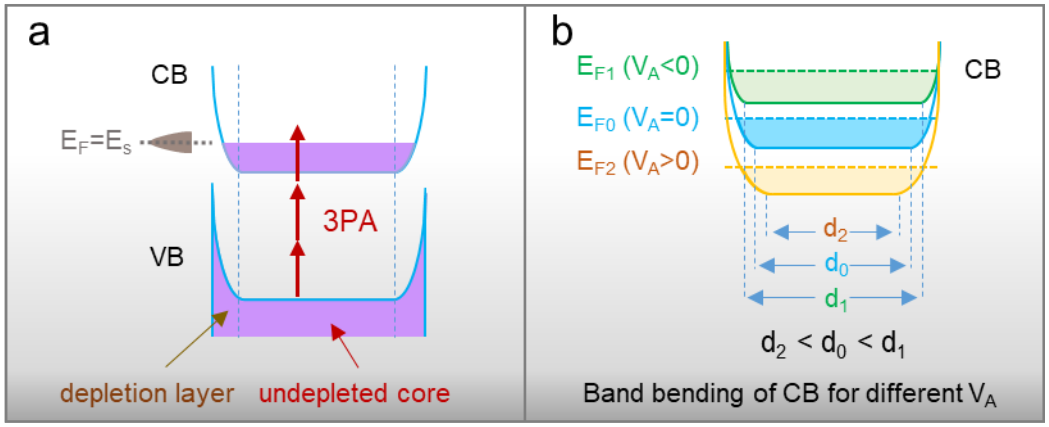

Figure 5. (a) Schematic of the band structure of ATO and the 3PA process. (b) Schematic of the conduction-band bending and diameter of the undepleted core corresponding to the different V_A values. VB is valence band, CB is conduction band, E_F is the Fermi potential, E_s is the surface state potential, and d is the diameter of the undepleted core. The subscripts 0, 1, and 2 refer to parameters corresponding to a V_A of 0, negative V_A, and positive V_A, respectively.

Linear absorption spectra (Figure 4a,b) show that the position of the LSPR peaks is nearly unchanged across the different voltages, while the peaks' intensities are V_A dependent. The insignificant variation in LSPR peak position with the charging and discharging of the conductive oxide has been attributed to the variation in the thickness of the surface depletion layer in ATO with the different voltages.[36,57,58] Surface defect states induce a depletion layer on the surface of the ATO nanoparticles (Figure 5a). The thickness of the depletion layer decreases with decreasing V_A (the charging of the ATO), and consequently the diameter of the undepleted core (d_1) increases (Figure 5b). In the present case, although the number of electrons increases because of charging, the increase in the carrier concentration in the undepleted core is

negligible, because the volume available to accommodate the electrons also increases due to depletion layer narrowing. For the discharging of ATO under a positive voltage, the electrons in the conduction band of ATO and the diameter of the undepleted core (d_2) both decrease, resulting in a negligible reduction in carrier concentration (i.e., the diameter of the undepleted core varies significantly with the applied voltage, but the electron concentration in the undepleted core does not). The frequency of the LSPR is associated with the carrier density in the undepleted core of ATO, while the intensity of the LSPR peak is determined by the amount of active material (*i.e.*, the undepleted core). Consequently, varying the V_A can influence the intensity of the LSPR but cannot significantly alter the peak position of the LSPR.

Z-scan experiments carried out with different laser intensities (Figure 1f) suggest that the nonlinear absorption corresponds to 3PA. The bandgap energy (E_g) of ATO derived from the Tauc plot of the UV-Vis-NIR absorption spectrum (Figure 1d) is 3.58 eV. From the energy perspective, the valence band maximum could be a ground state for 3PA, because the E_g value is smaller than three times the photon energy ($\hbar\omega$ = 1.20 eV) and larger than two times the photon energy. The linear absorption experiment (Figure 4) and the corresponding energy band model (Figure 5) show that the influence of V_A on the diameter of the undepleted core of the ATO nanoparticles is more significant than its effect on the carrier concentration in the conduction band. It is reasonable to ascribe the V_A-dependent γ_{eff} to the V_A-dependent diameter of the undepleted core of ATO. The charging of ATO results in a larger undepleted core, and therefore more active component for the 3PA process and a larger γ_{eff}, while the

discharging of the film leads to the shrinkage of the undepleted core, and a smaller γ_{eff}. 3PA from the depletion layer of the ATO nanoparticle is assumed to be negligible because the width of the depletion layer is relatively small compared to the diameter of the nanoparticle, due to the high doping level (~10%).[58] Because the depletion layer is relatively thin, the number of electrons in the valence band of the depletion region is small. The excitation associated with these electrons is susceptible to a ground-state depletion effect for which saturable absorption is expected.[59,60]

It should be noted that the strong saturable absorption (SA) associated with LSPR, which is usually found in highly doped semiconductors,[61,62] is negligible here. Strong SA at the LSPR peak results from abundant heat accumulation associated with resonant absorption at the LSPR peak, which shifts the resonance peak toward longer wavelengths and reduces the absorption at the initial wavelength. In our experiment, the laser wavelength (1030 nm) is far from the LSPR peak (~2300 nm), and so the absorption of laser photons is off-resonant, and the resultant heat accumulation is insufficient to induce the corresponding SA.

The PIL device has a larger modulation range of its linear and nonlinear transmittance than the IL device, suggesting a larger modulation of electron number in the conduction band of ATO in the PIL device. The different modulations of electron numbers in the PIL and the IL devices can be ascribed to the different amounts of H_2O impurities. Firstly, the activation of H_2O in the IL produces H^+ and OH^-, with smaller diameters than their counterpart ions in the IL (*i.e.*, $EMIM^+$ and BF_4^-), allowing adsorption of more ions on the surface of ATO than with the pure IL. In other words,

the capacitance of the PIL is larger than that of the pure IL due to a size effect of the ions.[49] Secondly, H^+ and OH^- can be electrochemically absorbed onto the surface of ATO.[49] The electrochemical absorption of H^+ and OH^- proceeds with a typical hysteresis effect, because of the energy barrier for the desorption of H^+ and/or OH^- from the surface of the ATO. Figure 2 and Figure 4 show that the hysteresis loop of the PIL device is much larger than that of the IL device, consistent with the electrochemical absorption of H^+ and OH^- being more prominent in the PIL device. As a consequence, the H_2O results in a larger effective capacitance of the electrical double layer at the interface of the ATO and IL, and a larger amount of H_2O impurity enables a larger modulation of the carrier concentration.

3. Conclusions

In summary, electrical tuning of the fifth-order optical nonlinearity of the ATO was demonstrated via ionic liquid gating. The ATO film shows tunable RSA behavior with 1030 nm 340 fs laser pulses. The γ_{eff} value can be electrically tuned between 0.51 and 3.46 cm^3 GW^{-2} using PIL as a dielectric, the enhancement factor being up to 6.8. The electrical modulation of γ_{eff} is attributed to the voltage-dependent size of the active component (*i.e.*, the undepleted core) in the ATO nanoparticles. The PIL affords a larger tuning range of γ_{eff} in comparison with the pure IL, because of its larger capacitance and electrochemical absorption of H^+ and OH^- on the surface of the ATO. In principle, the approach demonstrated in this work may be generally applicable to

other nonlinear materials, being an efficient and convenient procedure for the controlled tuning of nonparametric optical nonlinearity.

4. Experimental section

***Materials**:* FTO substrates (14 Ω sq^{-1}) were bought from Nippon Sheet Glass Co. Ltd., Japan. Antimony-doped (~ 10 at. %) tin oxide (ATO) nanoparticles were purchased from Beijing Shenghe Haoyuan Technology Co., Ltd. EMIM-BF_4 was purchased from Adamas Reagent, Ltd. Carbowax (2000) was supplied by Greagent Reagent, Ltd.

***Fabrication of ATO film**:* FTO substrate (2 × 2 cm^2) was initially cleaned by successive sonication in acetone, isopropanol, and methanol for 15 min each, subsequently rinsed with deionized (DI) water, and finally dried in a nitrogen stream. Afterwards, the FTO substrates were subjected to O_2 plasma treatment for 5 min. The ATO gel was prepared according to the method reported in Ref.[63]. In brief, ATO nanoparticles (0.75 g) were dispersed evenly into deionized water (4.3 mL) with the aid of an ultrasound probe (300 W, 4 h). Afterwards, Carbowax 20000 (0.6 g) was dissolved in the above solution, and then acetic acid (8 drops of 2 M solution) was added under stirring, resulting in a stable gel. The gel was homogeneously deposited onto the FTO substrate by the doctor blade method, and the redundant part was then wiped off, to leave a 1 × 1 cm^2 region of active material. After drying in air for 0.5 h, the gel film was annealed in air at 450 °C for 15 h.

Assembly of the device: With the ATO film as a working electrode, another FTO glass

(counter electrode) was mounted on top using a hot-melting Surlyn® membrane (60 μm thick) as a spacer and a binder. Afterwards, EMIM-BF_4 was then injected into the cavity of the device, and then the device was sealed with adhesive. The assembly of the device was carried out in a N_2-filled glove box.

Treatment of IL: Dehydration of the IL was undertaken using a sweeping method. [64] Briefly, N_2 gas (99.99%, 200 sccm) was bubbled through the IL (~ 1 mL) at 110 ºC for 5 h. The IL was then transferred into the glovebox for later use. The water content in the IL was measured by Karl Fischer titration (KLS-411, Micromoisture analyzer, Shanghai INESA Scientific Instrument Co., Ltd).

Characterization: The morphology of the ATO film was observed by an SEM (S-4800, Hitachi, Tokyo, Japan) operated at 5 kV. The structure of the films was characterized by XRD (Bruker D8 Advance) with Cu-Kα radiation (λ = 0.154178 nm). The TEM images were taken using a JEOL2100F operating at 200 kV. The UV-Vis-NIR spectra were recorded using a double-beam spectrophotometer (Cary 5000 UV-vis-NIR, Agilent Technologies). The application of voltages and CV measurements were carried out on an electrochemistry workstation (CHI 760E, CH Instrument)

Z-scan measurements: An open-aperture Z-scan setup was utilized to assess the NLO response of samples at different voltages. The laser source (FLCPA-03USPE11, Calmar laser, USA) generates a 1030 nm laser with a repetition rate of 1000 Hz and a pulse width of 340 fs for the Z-scan measurement. The laser beam was focused to a beam waist of 30 μm at the focal point.

Supporting Information

Supporting Information is available from the Wiley Online Library or from the author.

Acknowledgements

This research was financially supported by the National Natural Science Foundation of China (51772214, 51432006), the Ministry of Science and Technology of China (2011DFG52970), the Ministry of Education of China (IRT14R23), 111 Project (B13025), Jiangsu Province (2011-XCL-019 and 2013-479), and the Innovation Program of Shanghai Municipal Education Commission. M.G.H. and C.Z. thank the Australian Research Council for support (DP170100411).

Reference

[1] W. Cai, A. Vasudev, M. Brongersma, *Science* **2011**, *333*, 1720.

[2] L. Kang, Y. Cui, S. Lan, S. Rodrigues, M. Brongersma, W. Cai, *Nat. Commun.* **2014**, *5*, 4680.

[3] S. Lan, S. Rodrigues, Y. Cui, L. Kang, W. Cai, *Nano Lett.* **2016**, *16*, 5074.

[4] W. Ding, L. Zhou, S. Chou, *Nano Lett.* **2014**, *14*, 2822.

[5] J. Cox, Abajo, F. J. G. D., *Nat. Commun.* **2014**, *5*, 5725.

[6] K. T. Lee, M. Taghinejad, J. Yan, A. Kim, L. Raju, D. Brown, W. Cai, *ACS Photonics* **2019**, *6*, 2663.

[7] K. Seyler, J. Schaibley, P. Gong, P. Rivera, A. Jones, S. Wu, J. Yan, D. Mandrus,

W. Yao, X. Xu, *Nat. Nanotechnol.* **2015**, *10*, 407.

[8] Y. Wang, J. Xiao, H. Zhu, Y. Li, Y. Alsaid, K. Fong, Y. Zhou, S. Wang, W. Shi, Y. Wang, A. Zettl, E. Reed, X. Zhang, *Nature* **2017**, *550*, 487.

[9] J. Klein, J. Wierzbowski, A. Steinhoff, M. Florian, M. Rösner, F. Heimbach, K. Müller, F. Jahnke, T. Wehling, J. Finley, M. Kaniber, *Nano Lett.* **2017**, *17*, 392.

[10] G. Soavi, G. Wang, H. Rostami, D. Purdie, D. de Fazio, T. Ma, B. Luo, J. Wang, A. Ott, D. Yoon, S. Bourelle, J. Muench, I. Goykhman, S. Dal Conte, M. Celebrano, A. Tomadin, M. Polini, G. Cerullo, A. Ferrari, *Nat. Nanotechnol.* **2018**, *13*, 583.

[11] M. Ren, J. Berger, W. Liu, G. Liu, R. Agarwal, *Nat. Commun.* **2018**, *9*, 186.

[12] S. Chen, K. Li, G. Li, K. Cheah, S. Zhang, *Light Sci. Appl.* **2019**, *8*, 17.

[13] U. Keller, *Nature* **2003**, *424*, 831.

[14] Q. Guo, Y. Cui, Y. Yao, Y. Ye, Y. Yang, X. Liu, S. Zhang, X. Liu, J. Qiu, H. Hosono, *Adv. Mater.* **2017**, *29*, 1700754.

[15] C. Li, *Nonlinear Optics: Principles and Applications*, Springer, Harbin, China **2017**.

[16] G. Grinblat, R. Berte, M. Nielsen, Y. Li, R. Oulton, S. Maier, *Nano Lett.* **2018**, *18*, 7896.

[17] J. Wang, Y. Hernandez, M. Lotya, J. Coleman, W. Blau, *Adv. Mater.* **2009**, *21*, 2430.

[18] L. Tutt, T. Boggess, *Prog. Quant. Electron.* **1993**, *17*, 299.

[19] W. Zipfel, R. Williams, W. Webb, *Nat. Biotechnol.* **2003**, *21*, 1368.

[20] X. Liu, Q. Guo, J. Qiu, *Adv. Mater.* **2017**, *19*, 1605886.

[21] D. Dini, M. Calvete, M. Hanack, *Chem. Rev.* **2016**, *116*, 13043.

[22] J. Xu, X. Li, J. Xiong, C. Yuan, S. Semin, T. Rasing, X. Bu, *Adv. Mater.* **2020**, *32*, 1806736.

[23] G. Dalton, M. Cifuentes, S. Petrie, R. Stranger, M. Humphrey, M. Samoc, *J. Am. Chem. Soc.* **2007**, *129*, 11882.

[24] B. Babgi, L. Rigamonti, M. Cifuentes, T. Corkery, M. Randles, T. Schwich, S. Petrie, R. Stranger, A. Teshome, I. Asselberghs, K. Clays, M. Samoc, M. Humphrey, *J. Am. Chem. Soc.* **2009**, *131*, 10293.

[25] J. Jeong, N. Aetukuri, T. Graf, T. Schladt, M. Samant, S. Parkin, *Science* **2013**, *339*, 1402.

[26] K. Ueno, S. Nakamura, H. Shimotani, A. Ohtomo, N. Kimura, T. Nojima, H. Aoki, Y. Iwasa, M. Kawasaki, *Nat. Mater.* **2008**, *7*, 855.

[27] J. Ye, S. Inoue, K. Kobayashi, Y. Kasahara, H. Yuan, H. Shimotani, Y. Iwasa, *Nat. Mater.* **2010**, *9*, 125.

[28] J. Checkelsky, J. Ye, Y. Onose, Y. Iwasa, Y. Tokura, *Nat. Phys.* **2012**, *8*, 729.

[29] K. Shimamura, D. Chiba, S. Ono, S. Fukami, N. Ishiwata, M. Kawaguchi, K. Kobayashi, T. Ono, *Appl. Phys. Lett.* **2012**, *100*, 122402.

[30] Y. Yamada, K. Ueno, T. Fukumura, H. Yuan, H. Shimotani, Y. Iwasa, L. Gu, S. Tsukimoto, Y. Ikuhara, M. Kawasaki, *Science* **2011**, *332*, 1065.

[31] M. Moser, G. Li, M. Chen, E. Bekyarova, M. Itkis, R. Haddon, *Nano Lett.* **2016**, *16*, 5386.

[32] Z. Wu, Z. Chen, X. Du, J. Logan, J. Sippel, M. Nikolou, K. Kamaras, J. Reynolds, D. Tanner, A. Hebard, A. Rinzler, *Science* **2004**, *305*, 1273.

[33] M. Shkir, S. AlFaify, *Sci. Rep.* **2017**, *7*, 16091.

[34] M. Shkir, V. Ganesh, S. AlFaify, I. Yahia, H. Zahran, *J Mater Sci: Mater Electron* **2018**, *29*, 6446.

[35] A. Moholkar, S. Pawar, K. Rajpure, C. Bhosale, *J. Alloy. Compd.* **2008**, *455*, 440.

[36] U. Felde, M. Haase, H. Weller, *J. Phys. Chem. B* **2000**, *104*, 9388.

[37] D. Corrêa, L. de Boni, L. Misoguti, I. Cohanoschi, F. Hernandez, C. Mendonça, *Opt. Commun.* **2007**, *277*, 440.

[38] Q. Zhang, X. Liu, M. Utama, G. Xing, T. Sum, Q. Xiong, *Adv. Mater.* **2016**, *28*, 276.

[39] J. He, Y. Qu, H. Li, J. Mi, W. Ji, *Opt. Exp.* **2005**, *13*, 9235.

[40] J. He, W. Ji, J. Mi, Y. Zheng, J. Ying, *Appl. Phys. Lett.* **2006**, *88*, 181114.

[41] J. He, G. Scholes, Y. Ang, W. Ji, C. Beh, W. Chin, *Appl. Phys. Lett.* **2008**, *92*, 131114.

[42] M. Vivas, T. Shih, T. Voss, E. Mazur, C. Mendonca, *Opt. Exp.* **2010**, *18*, 9628.

[43] M. Cifuentes, C. Powell, M. Humphrey, G. Heath, M. Samoc, B. Luther-Davies, *J. Phys. Chem. A* **2001**, *105*, 9625.

[44] C. Powell, M. Humphrey, M. Cifuentes, J. Morrall, M. Samoc, B. Luther-Davies, *J. Phys. Chem. A* **2003**, *107*, 11264.

[45] C. Powell, M. Cifuentes, J. Morrall, R. Stranger, M. Humphrey, M. Samoc, B. Luther-Davies, G. Heath, *J. Am. Chem. Soc.* **2003**, *125*, 602.

[46] M. Cifuentes, C. Powell, J. Morrall, A. McDonagh, N. Lucas, M. G. Humphrey, M. Samoc, S. Houbrechts, I. Asselberghs, K. Clays, A. Persoons, T. Isoshima, *J. Am. Chem. Soc.* **2006**, *128*, 10819.

[47] S. Hurst, M. Cifuentes, J. Morrall, N. Lucas, I. Whittall, M. Humphrey, I. Asselberghs, A. Persoons, M. Samoc, B. Luther-Davies, A. Willis, *Organometallics* **2001**, *20*, 4664.

[48] Q. Feng, Y. Li, G. Shi, L. Wang, W. Zhang, K. Li, H. Hou, Y. Song, *J. Mater. Chem. C* **2016**, *4*, 8552.

[49] H. Yuan, H. Shimotani, A. Tsukazaki, A. Ohtomo, M. Kawasaki, Y. Iwasa, *J. Am. Chem. Soc.* **2010**, *132*, 6672.

[50] R. Subbaraman, D. Tripkovic, D. Strmcnik, K.-C. Chang, M. Uchimura, A. Paulikas, V. Stamenkovic, N. Markovic, *Science* **2011**, *334*, 1256.

[51] T. Schladt, T. Graf, N. Aetukuri, M. Li, A. Fantini, X. Jiang, M. Samant, S. Parkin, *ACS Nano* **2013**, *7*, 8074.

[52] J. Jeong, N. Aetukuri, T. Graf, T. Schladt, M. Samant, S. Parkin, *Science* **2013**, *339*, 1402.

[53] H.-J. Jeon, M.-K. Jeon, M. Kang, S.-G. Lee, Y.-L. Lee, Y.-K. Hong, B.-H. Choi, *Mater. Lett.* **2005**, *59*, 1801.

[54] L. Yang, J. Huang, L. Shi, L. Cao, W. Zhou, K. Chang, X. Meng, G. Liu, Y. Jie, J. Ye, *Nano Energy* **2017**, *36*, 331.

[55] P. Pattathil, R. Giannuzzi, M. Manca, *Nano Energy* **2016**, *30*, 242.

[56] G. Garcia, R. Buonsanti, E. Runnerstrom, R. Mendelsberg, A. Llordes, A. Anders,

T. Richardson, D. Milliron, *Nano Lett.* **2011**, *11*, 4415.

[57] A. Agrawal, I. Kriegel, E. Runnerstrom, F. Scotognella, A. Llordes, D. Milliron, *ACS Photonics* **2018**, *5*, 2044.

[58] O. Zandi, A. Agrawal, A. Shearer, L. Reimnitz, C. Dahlman, C. Staller, D. Milliron, *Nat. Mater.* **2018**, *17*, 710.

[59] M. Barroso, S. Pendlebury, A. Cowan, J. Durrant, *Chem. Sci.* **2013**, *4*, 2724.

[60] M. Sachs, J.-S. Park, E. Pastor, A. Kafizas, A. Wilson, L. Francàs, S. Gul, M. Ling, C. Blackman, J. Yano, A. Walsh, J. Durrant, *Chem. Sci.* **2019**, *10*, 5667.

[61] M. Alam, I. de Leon, R. Boyd, *Science* **2016**, *352*, 795.

[62] Q. Guo, Y. Cui, Y. Yao, Y. Ye, Y. Yang, X. Liu, S. Zhang, X. Liu, J. Qiu, H. Hosono, *Adv. Mater.* **2017**, *29*, 1700754.

[63] G. Boschloo, D. Fitzmaurice, *J. Phys. Chem. B* **1999**, *103*, 3093.

[64] S. Ren, Y. Hou, W. Wu, W. Liu, *J. Chem. Eng. Data* **2010**, *55*, 5074.

The fifth order optical nonlinearity of antimony-doped tin oxide (ATO) is electrically modulated by external bias, with enhancement as large as 6.8-fold. The electrical modulation is ascribed to the voltage-dependent radius of the undepleted core of the ATO. A smaller voltage results in the charging of the ATO and a larger undepleted core, and the size of the active component for three-photon absorption is larger.

Ruipeng Hou, Hui Li, Yanhui Sun, Mengjuan Diao, Ying Liang, Zhipeng Huang,*
Jun Wang, Mark G. Humphrey, and Chi Zhang*

Electrical Tuning of the Fifth-Order Optical Nonlinearity of Antimony-Doped Tin Oxide